

Article

## Biofuels Produced by Fischer-Tropsch Synthesis over Silica-supported Iron-Based Catalysts Prepared by Autocombustion Method

Suthasinee Pengnarapat<sup>1,2,a</sup>, Tharapong Vitidsant<sup>1,2,b,\*</sup>, Noritatsu Tsubaki<sup>3,c</sup>,  
Prasert Reubroycharoen<sup>1,d</sup>, and Jaru Natakaranakul<sup>1,2,e</sup>

<sup>1</sup> Department of Chemical Technology, Faculty of Science, Chulalongkorn University, Bangkok 10330, Thailand

<sup>2</sup> Centre of Fuel and Energy from Biomass, Faculty of Science, Chulalongkorn University, Saraburi 18110, Thailand

<sup>3</sup> Department of Applied Chemistry, School of Engineering, University of Toyama, Gofuku 3190, Toyama 930-8555, Japan

E-mail: <sup>a</sup>suthasinee.pe@chula.ac.th, <sup>b,\*</sup>tharapong.v@chula.ac.th (Corresponding authors), <sup>c</sup>tsubaki@eng.u-toyama.ac.jp, <sup>d</sup>prasert.r@chula.ac.th, <sup>e</sup>jaru.nara@gmail.com

**Abstract.** The purpose of this study was to evaluate the effect of different silica types on iron (Fe)-based catalysts containing copper and potassium prepared by autocombustion for direct use in Fischer-Tropsch Synthesis (FTS) without a reduction step. The catalysts were characterized through nitrogen (N<sub>2</sub>) adsorption, X-ray diffraction (XRD), and transmission electron microscopy (TEM). The FTS performance of each catalyst was evaluated in a fixed-bed reactor at 300 °C, 1.0 MPa, a catalyst weight to volume flow rate of 10 g<sub>cat</sub> h/mol and a hydrogen (H<sub>2</sub>)/carbon monoxide (CO) molar ratio of 1. The pore size of the silica had an important influence on the formation of the Fe active phases and subsequent FTS activity. The presence of iron carbide (Fe<sub>x</sub>C), which is known to be one of the active Fe phases, was demonstrated by the XRD and TEM analyses. Larger crystallite sizes in the large pores were much easier to accommodate Fe<sub>x</sub>C than the smaller crystallite sizes in the small pores. The Fe-based catalysts supported on the silica with the largest pores gave the highest CO conversion level at 86.5%, with a 28.1% C<sub>2-4</sub> selectivity and 17.3% C<sub>5+</sub> selectivity under these operating conditions. Interestingly, this is an alternative approach to synthesize nanostructured metallic catalysts on silica and to produce clean biofuel for the fuel industry and transportation.

**Keywords:** Fischer-Tropsch synthesis, Silica, Fe-based catalysts, autocombustion method, biofuel.

**ENGINEERING JOURNAL** Volume 25 Issue 4

Received 4 December 2020

Accepted 29 December 2020

Published 30 April 2021

Online at <https://engj.org/>

DOI:10.4186/ej.2021.25.4.87

*This article is based on the presentation at The 29th Thai Institute of Chemical Engineering and Applied Chemistry Conference (TICbE 2020) in Bangkok, 1st-2nd June 2020.*

## 1. Introduction

Fischer-Tropsch synthesis (FTS), for altering syngas into liquid fuels and chemicals, is an important technology in the conversion of coal, natural gas, and biomass to liquid products [1]. Iron (Fe)-based catalysts are preferred for the FTS reaction due to their low cost, high activity, and excellent water gas shift (WGS) reactivity, which are advocated for the conversion of syngas from coal gasification with a low hydrogen (H<sub>2</sub>)/carbon monoxide (CO) ratio [2]. To achieve a high performance, copper (Cu) is frequently added to the Fe to realize a lower reduction temperature and reduce the level of sintering. Furthermore, Fe-based catalysts need an alkali metal, such as potassium (K), as a chemical promoter to enhance both the FTS and WGS activity and increase the selectivity for the long chain hydrocarbons (HCs) [3].

In order to improve the FTS performance, structural promoters are necessary additives in industrial Fe-based catalysts. The role of silica (SiO<sub>2</sub>) for Fe-based catalysts in the FTS is generally regarded to be physical in nature, in terms of providing a large surface area, stabilizing small Fe crystallites sizes, and enhancing the attrition resistance of catalysts [4, 5]. As generally known, the textural properties of the silica have a great influence on the catalytic performances since it affects the active particle sizes and dispersion. A high dispersion of Fe oxide particles enhances the heat and mass transfer as well as giving a high resistance against coke formation and deposition [6].

Autocombustion is an alternative synthesis method that uses energy from the exothermic decomposition of a redox mixture of organic acid and metal nitrates. The reducing gases, such as H<sub>2</sub> and CO, are released from the exothermic decomposition of the organic acid and then reduce the metal ions to active metal. Therefore, this process can continue without an external energy source. This approach has the advantage of a low cost and high energy performance. There have been several reports on the preparation of catalysts by autocombustion [7]. For example, a series of the cobalt-based catalysts on silica were formed from autocombustion using cobalt nitrates and citric acid in an argon (Ar) atmosphere. Increasing the citric acid level increased the degree of reduction and extended the cobalt dispersion, but markedly increased the level of carbon residues [8].

With respect to catalysts for the FTS, Fe-based FTS catalysts containing Cu and K and supported on silica, were prepared by autocombustion of citric acid for direct use in the FTS reaction without a reduction step [9]. The optimal catalyst, in terms of the highest CO conversion level, was obtained with a citric acid: iron (III) nitrate molar ratio of 0.1, and was superior to the corresponding catalysts prepared by impregnation [9].

However, Fe-based catalysts for FTS on different silica types prepared by autocombustion have not been reported in detail. It is of great interesting and challenging to improve catalysts that are comprised of different types of silica supports. Consequently, the objective of this study was focused on the influence of Fe-based catalysts

containing Cu, K and citric acid that were supported on different silica types and prepared by autocombustion for direct FTS without a reduction step. The catalysts were characterized through nitrogen (N<sub>2</sub>) adsorption, X-ray diffraction (XRD), and transmission electron microscopy (TEM). The effect of different silica types on the FTS performance of catalysts were tested in a fixed-bed reactor and correlated with the characterization results.

## 2. Experimental

### 2.1. Catalyst Preparation

The Fe-based catalysts containing Cu, K and citric acid and supported on silica were prepared by autocombustion as previously described [9, 10], using iron (III) nitrate nonahydrate, copper (II) nitrate trihydrate, and potassium nitrate at a Fe: Cu: K molar ratio of 200:30:5 and citric acid. The respective chemicals were initially dissolved in distilled water to give a citric acid: iron nitrate molar ratio of 0.1. The solutions were adjusted to pH 7.0 using ammonia (NH<sub>3</sub>) solution, refluxed at 80 °C for 2 h and then evaporated at 100 °C until a dark brown solution of 25 cm<sup>3</sup>. The supports were the commercially available Q-3, Q-10, and Q-50 silica (Cariact, Fuji Silysia Co. Ltd.). The Fe/Cu/K mixture was then impregnated over the silica (5 g) at a 20 wt% Fe metal loading and dried at 120 °C for 12 h. The resulting samples were calcined in Ar at 500 °C for 5 h at a ramping rate of 1.5 °C/min and then applied directly in the FTS without a reduction step. The Q-3, Q-10, and Q-50 supported FeCuK catalysts were denoted as FeCuK/Q-3, FeCuK/Q-10, and FeCuK/Q-50, respectively.

### 2.2. Catalyst Characterization

The pore structure of calcined catalysts was characterized by nitrogen (N<sub>2</sub>) adsorption using a NOVA 2200e equipment. The specific surface area ( $S_{\text{BET}}$ ) was obtained by the Brunauer-Emmett-Teller (BET) method, the total pore volume ( $V_p$ ) was calculated by the single point method, and the average pore sizes ( $D_p$ ) was obtained by  $4V_p/S_{\text{BET}}$ . The pore size distribution (PSD) was obtained using the Barrett-Joyner-Halenda (BJH) method. The XRD patterns of calcined and used catalysts were performed using a Rigaku RINT 2200 with a monochromatic Cu-K $\alpha$  radiation source over a  $2\theta$  range from 10–80°. The Scherrer equation,  $D = K\lambda/(\beta\cos\theta)$  was used to calculate the average crystalline sizes of calcined and used catalysts. The TEM images were analysed by a Philips Tecnai F20 TEM at 200 kV acceleration voltage and field emission source which was equipped with digital STEM. The average crystallite sizes of used catalyst were calculated by the SemAfore program.

### 2.3. Catalyst Activity Test

The feed gas for FTS consisted of Ar (3.0%), CO (48.5%), and H<sub>2</sub> (48.5%). Initially, the respective catalyst

(0.5 g) was placed in a fixed bed reactor tube. Thereafter, the FTS reaction was performed for 6 h at 300 °C, 1.0 MPa and a  $W/F$  ratio of 10  $\text{g}_{\text{cat}} \text{ h/mol}$ . The stream was characterized by online gas chromatography (GC) as follows: a thermal conductivity detector (TCD) was used to analyse the gaseous products [methane ( $\text{CH}_4$ ), carbon dioxide ( $\text{CO}_2$ ), CO, and Ar] and a flame ionization detector (FID) was used to evaluate the light HCs ( $\text{C}_1$ – $\text{C}_5$ ). The liquid products were collected in an ice trap and analysed by GC-FID. The experimental set up is shown schematically in Fig. 1.

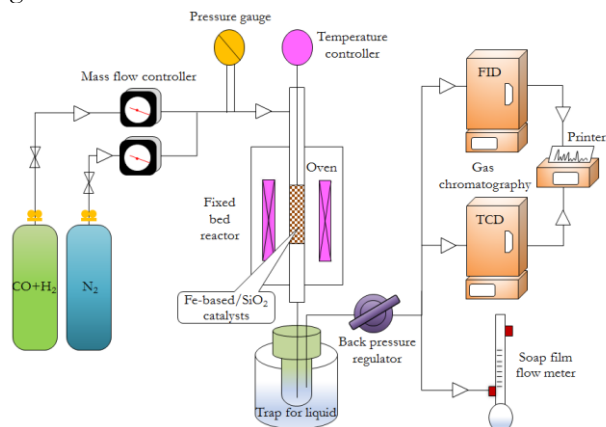


Fig. 1. Schematic diagram of the FTS apparatus used in this study.

### 3. Results and Discussion

#### 3.1. Textural Characteristics of Catalysts

Table 1. Physical properties of the three silica types, and their derived as-synthesized FeCuK catalysts.

Material	$S_{\text{BET}}^a$ ( $\text{m}^2/\text{g}$ )	$V_p^a$ ( $\text{cm}^3/\text{g}$ )	$D_p^a$ (nm)
Q-3	760	0.35	4.6
FeCuK/Q-3	661	0.19	3.2
Q-10	475	1.53	13.4
FeCuK/Q-10	446	0.96	10.7
Q-50	80	1.10	48.5
FeCuK/Q-50	92	0.57	20.2
Q-3	760	0.35	4.6
FeCuK/Q-3	661	0.19	3.2
Q-10	475	1.53	13.4

<sup>a</sup> Determined by the  $\text{N}_2$  adsorption method.

For comparison of the effect of different silica types, the catalysts with the same composition but using the Q-3, Q-10, or Q-50 silica as the support were examined. Thus, the physical properties of the calcined FeCuK/Q-3, FeCuK/Q-10, and FeCuK/Q-50 catalysts were determined by  $\text{N}_2$  adsorption, with the results summarized in Table 1. The  $S_{\text{BET}}$  of the Q-3 and Q-10 silica was reduced in the respective FeCuK/Q-3 and FeCuK/Q-10 catalysts from 760 to 661  $\text{m}^2/\text{g}$  and from 475 to 446  $\text{m}^2/\text{g}$ , respectively. This indicated that the introduced components may be deposited on the entrance of large pores and so block them. In contrast, the  $S_{\text{BET}}$  of the Q-

50 silica was slightly increased upon formation of the FeCuK/Q-50 catalyst from 80 to 92  $\text{m}^2/\text{g}$ , mainly due to some Fe particles entering into the pores of the silica [10, 11]. The citric acid in the Fe-based catalysts released gases during the citric acid decomposition that resulted in a more porous structure and higher  $S_{\text{BET}}$ .

Likewise, the  $V_p$  of Q-3 was decreased from 0.35 to 0.19  $\text{cm}^3/\text{g}$  in the FeCuK/Q-3 catalyst, while for Q-10 it was decreased from 1.53 to 0.96  $\text{cm}^3/\text{g}$  in the FeCuK/Q-10 catalyst, indicating that some of the introduced metal species entered the small pores of the Q-3 and Q-10 silica support [12]. In contrast to the  $S_{\text{BET}}$ , the  $V_p$  of Q-50 was also markedly decreased from 1.1 to 0.57  $\text{cm}^3/\text{g}$  in the FeCuK/Q-10 catalyst (Table 1). The  $D_p$  of the Q-3, Q-10, and Q-50 silicas were all decreased upon formation of their respective FeCuK catalyst by autocombustion and calcination, in accord with a previous study [12]. This marked decrease in the  $V_p$  and  $D_p$  suggests that the Fe particles were loaded into the pores of silica more than deposited on the outer surface. As expected, it was noted that the silica helped to protect the Fe-based catalysts on the silica matrix during the calcination step, absorbing the heat from the autocombustion and so avoiding structure collapse [13].

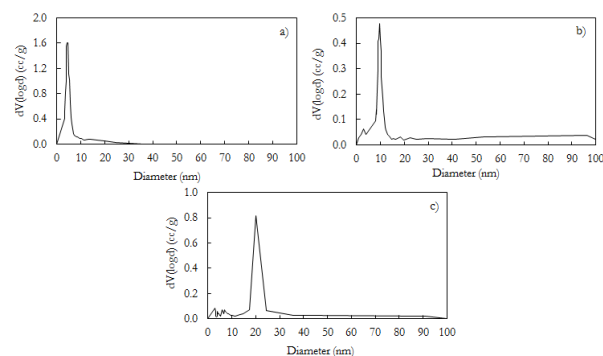


Fig. 2. Plots of the PSD of the (a) FeCuK/Q-3, (b) FeCuK/Q-10, and (c) FeCuK/Q-50 catalysts.

The pore size distributions (PSD) of the calcined catalysts are shown in Fig. 2. The samples prepared from the different silica types all had a uniform pore size with a very narrow PSD between 2 and 25 nm, as calculated using the BJH method for the mesoporous silica [4]. The FeCuK/Q-3 catalyst, with a very high surface area and relatively narrow mesopores, showed a smaller pore diameter in the PSD curve than the other two catalysts, as expected [2]. It should be noted that the PSD curve of the FeCuK/Q-50 catalyst was broader (17–25 nm), with a maximum at about 20 nm, than those for FeCuK/Q-3 and FeCuK/Q-10.

#### 3.2. Crystalline Structures of the Catalysts

The metal dispersion on the silica supports was evaluated from the XRD patterns of the calcined FeCuK/Q-3, FeCuK/Q-10, and FeCuK/Q-50 catalysts before FTS, and are shown in Fig. 3(a). The calcined catalysts exhibited the presence of Fe in hematite ( $\text{Fe}_2\text{O}_3$ ),

magnetite ( $\text{Fe}_3\text{O}_4$ ), and carbides ( $\text{Fe}_x\text{C}$ ) phases. The broad peak observed at a  $2\theta$  range from  $20\text{--}25^\circ$  corresponded to amorphous silica. The XRD patterns were very broad, especially for the FeCuK/Q-3 catalyst, which indicated a relatively small crystalline size. The width of the XRD peaks of  $\text{Fe}_3\text{O}_4$  were apparent in the FeCuK/Q-50 catalyst and were strongly affected by the pore size. No XRD peaks were assigned to Cu or K species due to their high dispersion level and low concentration [9]. Increasing the pore size caused a further reduction of  $\text{Fe}_2\text{O}_3$  to  $\text{Fe}_3\text{O}_4$  and then carburization of Fe metal (Fe) to  $\text{Fe}_x\text{C}$ . Consequently, the autocombustion process completed the conversion of metal compounds to metal oxides and then to metal carbides without a reduction step [14].

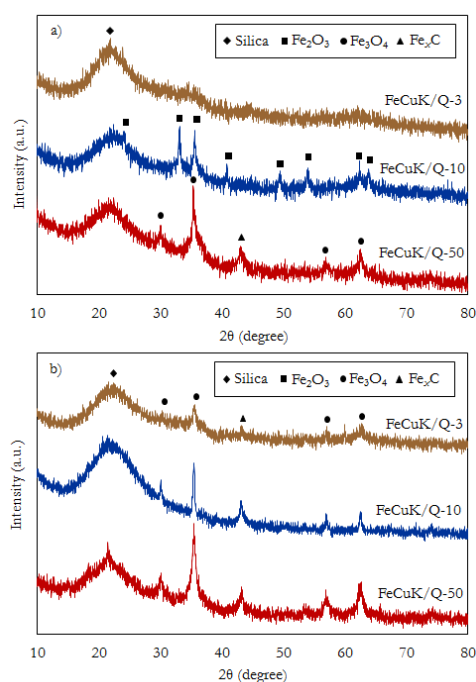


Fig. 3. XRD patterns of the FeCuK/Q-3, FeCuK/Q-10, and FeCuK/Q-50 catalyst (a) before and (b) after a 6-h FTS reaction.

The as-synthesized FeCuK/Q-50 catalyst revealed the presence of a  $\text{Fe}_x\text{C}$  phase, as seen in Fig. 3(a). This carburization might have occurred during the calcination step in the catalyst preparation process, where the citric acid was used as the reducing agent and iron nitrate as the oxidizing agent. The decomposition of citric acid releases large amounts of gases, such as  $\text{H}_2$ ,  $\text{CH}_4$ ,  $\text{H}_2\text{O}$ ,  $\text{CO}$ ,  $\text{CO}_2$ ,  $\text{NH}_3$ , nitrogen dioxide ( $\text{NO}_2$ ), and nitrogen monoxide ( $\text{NO}$ ). The reducing  $\text{H}_2$  and  $\text{CO}$  would then play a key role as the reducing and carburizing agents to produce  $\text{Fe}_x\text{C}$  from the metal oxides phases [14], as showed in Fig. 4.

Figure 3(b) displayed the XRD patterns of used catalysts after the 6-h FTS reaction. The XRD patterns of all catalysts showed Fe phases as  $\text{Fe}_3\text{O}_4$  and  $\text{Fe}_x\text{C}$ . Increasing silica pore sizes led to a gradual increased intensity of  $\text{Fe}_x\text{C}$ , as observed from the average crystallite sizes calculated by the Scherrer formula in Table 2. After the 6-h FTS reaction, the FeCuK/Q-50 catalyst contained more  $\text{Fe}_x\text{C}$  than the FeCuK/Q-3 and FeCuK/Q-10

catalysts. The intensities of these peaks were larger with the large pore sized catalysts, with a higher  $\text{Fe}_x\text{C}$  amount [2]. This is consistent with the XRD patterns for the calcined FeCuK/Q-3, FeCuK/Q-10, and FeCuK/Q-50 catalysts in Fig. 3(a). It is worth noting that the carburization of small iron oxide particles led to a small level of  $\text{Fe}_x\text{C}$ , and so the Fe dispersion in silica was influenced by the pore size of the silica [4].

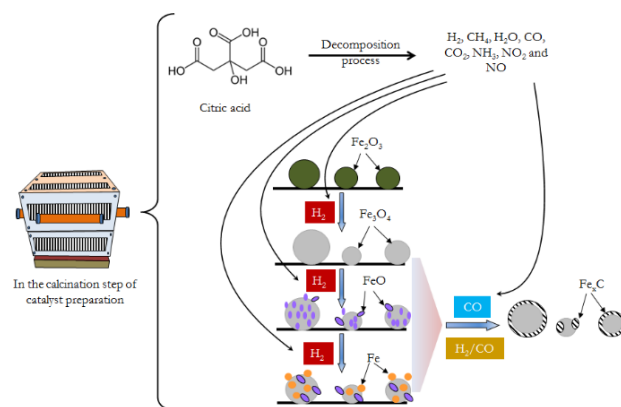


Fig. 4. Schematic diagram showing the carburization and transformation sequence for Fe phase the calcination catalyst preparation [14].

The crystalline sizes of the FeCuK/Q-3, FeCuK/Q-10, and FeCuK/Q-50 catalysts are summarized in Table 2. Increasing the pore size resulted in narrowing XRD peaks and in larger sizes of  $\text{Fe}_2\text{O}_3$  and  $\text{Fe}_3\text{O}_4$  crystallites. Moreover, the crystallite sizes followed the same trend as the silica pore sizes, where larger crystallite sizes were located in larger pore sizes, as reported previously [4], especially in the FeCuK/Q-50 catalyst, as seen in Fig. 3(a).

Table 2. The crystalline sizes of the FeCuK/Q-3, FeCuK/Q-10, and FeCuK/Q-50 catalysts.

Catalyst	$d_{\text{XRD}}^{\text{a}}$ (nm)		$d_{\text{TEM}}^{\text{d}}$ (nm)
	Calcined <sup>b</sup>	Used <sup>c</sup>	
FeCuK/Q-3	4.8	7.1	7.6
FeCuK/Q-10	17.7	12.4	15.8
FeCuK/Q-50	27.5	14.8	19.2

<sup>a</sup>Derived from the diffraction line in XRD and the crystalline sizes calculated by the Scherrer formula; <sup>b</sup> $\text{Fe}_2\text{O}_3$  at  $35.5^\circ$  and  $\text{Fe}_3\text{O}_4$  at  $35.3^\circ$  for calcined catalysts before FTS; <sup>c</sup> $\text{Fe}_x\text{C}$  at around  $43.0^\circ$  for used catalysts after FTS. <sup>d</sup> $\text{Fe}_x\text{C}$  sizes for used catalysts after a 6-h FTS reaction, as derived from the TEM analysis.

### 3.3. Morphology (TEM analysis) of the Catalysts

Representative TEM images of the used (after the 6-h FTS reaction) FeCuK/Q-3, FeCuK/Q-10, and FeCuK/Q-50 catalysts are compared in Fig. 5. All the TEM images were broadly similar [4], and showed the effect of the silica pore size on the dispersion of the  $\text{Fe}_x\text{C}$  phase in the used catalysts. As expected, more dispersed  $\text{Fe}_x\text{C}$  species were observed in the smaller pore sizes.

Table 2 shows the average crystallite sizes of the  $\text{Fe}_x\text{C}$  phase of the used catalysts, as calculated using the SemAfore program. The average crystallite sizes of  $\text{Fe}_x\text{C}$  increased initially from 7.6 nm to 15.8 nm and then markedly to 19.2 nm, as the pore size of silica increased from those in Q-3 to Q-10 and then to Q-50, respectively. In accord, increasing the pore size increased the average crystallite size of  $\text{Fe}_x\text{C}$ . The result revealed that a more dispersed  $\text{Fe}_x\text{C}$  phase was observed in the Q-50 silica with larger pore sizes [6], which is in accord with the XRD data in Fig. 3(b), where the intensity of  $\text{Fe}_x\text{C}$  peaks appeared in the used FeCuK/Q-3, FeCuK/Q-10, and FeCuK/Q-50 catalysts after the 6-h FTS reaction.

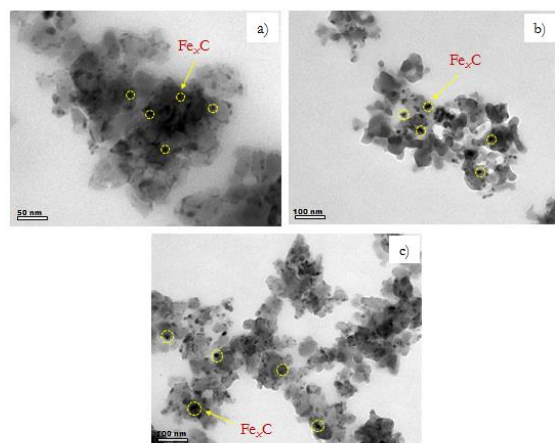


Fig. 5. TEM images of the used (after a 6-h FTS reaction) (a) FeCuK/Q-3, (b) FeCuK/Q-10, and (c) FeCuK/Q-50 catalysts.

### 3.4. FTS Performance

#### 3.4.1. CO conversion

Table 3. The FTS<sup>a</sup> performance, in terms of the CO conversion efficiency and product selectivity, of the FeCuK/Q-3, FeCuK/Q-10, and FeCuK/Q-50 catalysts.

Catalyst	CO conversion	Product selectivity (%)			
		CO <sub>2</sub>	CH <sub>4</sub>	C <sub>2-4</sub>	C <sub>5+</sub>
FeCuK/Q-10	10.8	28.8	45.7	15.9	9.6
FeCuK/Q-10	33.3	35.7	24.2	25.2	14.9
FeCuK/Q-50	86.5	37.8	16.8	28.1	17.3

<sup>a</sup> Reaction condition: 0.5 g catalyst, H<sub>2</sub>/CO of 1/1, 300 °C, 1.0 MPa, and W/F = of 10 g<sub>cat</sub> h/mol.

The calcined FeCuK/Q-3, FeCuK/Q-10, and FeCuK/Q-50 catalysts were used in the FTS reaction to investigate the promotional role of the silica pore structure. The obtained CO conversion level and product selectivity are summarized in Table 3. Comparing the FeCuK/Q-3 and FeCuK/Q-50 catalysts, the former catalyst with the largest surface area (661 m<sup>2</sup>/g) and smallest average pore size (3.2 nm) showed the lowest CO conversion level, whereas the latter catalyst with the smallest surface area (92 m<sup>2</sup>/g) and largest pore size (20.2 nm) showed a higher CO conversion level. Therefore, increasing the silica pore

size increased the CO conversion level to a maximum of 86.5% in this study, being ranked in the order FeCuK/Q-50 > FeCuK/Q-10 > FeCuK/Q-3.

It is important to note that the pore size of the silica support for the FeCuK catalysts played a more important role than the surface area on the CO conversion level [12]. The reaction rate is likely to be mainly controlled by the diffusion of reactants and products. The CO conversion level compared to the catalyst pore size ( $D_p$ ) are compared in Fig. 6. As expected, the CO conversion level increased as a function of the silica pore size. In accord, the noted trend was that a much higher CO conversion level was obtained with a larger pore size of silica [4]. Indeed, several previous reports showed that a higher CO conversion level in the FTS reaction depended on the faster diffusion rate /greater efficiency and the improved active metal dispersion [2, 12].

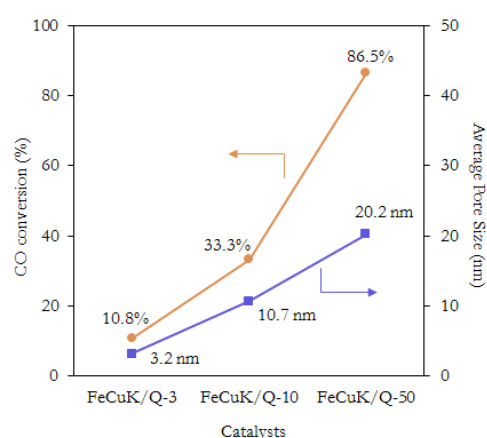


Fig. 6. The CO conversion level obtained in the FTS reaction with the FeCuK/Q-3, FeCuK/Q-10, and FeCuK/Q-50 catalysts, and their respective pore sizes ( $D_p$ ).

Moreover, it should be noted that the FeCuK/Q-50 catalyst had the highest CO conversion level in this FTS reaction. Two main factors may be associated with this improvement. Firstly, as is indicated by XRD patterns of the calcined catalysts (Fig. 3(a)), the FeCuK/Q-50 catalyst contained  $\text{Fe}_3\text{O}_4$ , which can be readily converted by carburization of Fe to  $\text{Fe}_x\text{C}$ . A larger amount of  $\text{Fe}_x\text{C}$  would result, which is the true active species for FTS. Secondly, the XRD patterns of the used catalysts (after the 6-h FTS reaction) revealed that the FeCuK/Q-50 catalyst contained more  $\text{Fe}_x\text{C}$  than the other two catalysts (Fig. 3(b)). The TEM results (Table 2) of the used catalysts also confirmed that the FeCuK/Q-50 catalyst had a higher  $\text{Fe}_x\text{C}$  content than the other two catalysts [12].

It is interesting that the CO conversion level of these three FeCuK/SiO<sub>2</sub> catalysts synthesized by autocombustion remained almost unchanged over the 6-h FTS reaction, as exhibited in Fig. 7. It was deduced that Fe carburization and stability were achieved by surface active carbonaceous species during the preparation of the catalysts in the autocombustion method [15]. Consequently, the induction period required for conventional Fe-based catalysts for the FTS was not

necessary for these catalysts synthesized by autocombustion. As expected, the existence of citric acid significantly improved the reduction and carburization of iron oxide phases during catalyst preparation, which suggested that this carbonaceous material worked as reducing agent during the decomposition of nitrate to form partially reduced Fe species. Similar results have been reported before, where the addition of carbonaceous material into the precursors led to the stabilization of highly dispersed iron oxide phases and a more reduced active phase after heat treatment in an inert atmosphere [16].

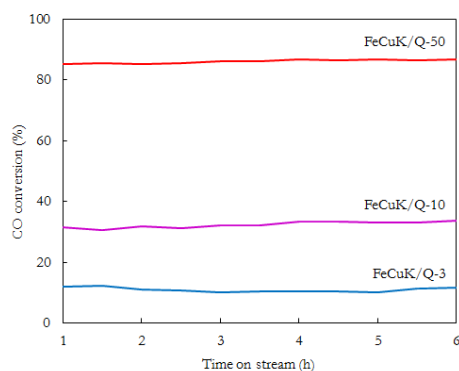


Fig. 7. Plot showing the influence of the FeCuK/Q-3, FeCuK/Q-10, and FeCuK/Q-50 catalysts on the CO conversion level over a 6-h FTS reaction. Reaction condition: 0.5 g catalyst, H<sub>2</sub>/CO of 1/1, 300 °C, 1.0 MPa, and a W/F of 10 g<sub>cat</sub> h/mol.

### 3.4.2. Product selectivity

The product selectivity during the 6-h FTS reaction of citric acid with the three different catalyst types are shown in Table 3 and Fig. 8. The reaction product selectivity was influenced by the average pore and crystallite sizes. Since Fe-based catalysts in the FTS commonly have a high WGS reaction activity, then the CO<sub>2</sub> selectivity was presumably mainly derived from the WGS reaction [17]. The FeCuK/Q-50 catalyst had the highest CO<sub>2</sub> selectivity, where increasing the silica support pore size significantly increased the CO<sub>2</sub> selectivity, which is because the WGS reaction was catalysed by the Fe<sub>3</sub>O<sub>4</sub> phase. Accordingly, a higher Fe<sub>3</sub>O<sub>4</sub> phase could lead to high CO<sub>2</sub> selectivity [18].

Comparison between the FeCuK/Q-3 and FeCuK/Q-50 catalysts revealed that FeCuK/Q-3 showed a higher CH<sub>4</sub> selectivity, due to the influence of the pore size, where increasing the pore size led to a strongly decreased CH<sub>4</sub> selectivity. Small pores would contribute to the formation of small molecular weight products from the diffusion limitation, while large pores benefited the formation of heavy HCs. The stronger -CH<sub>x</sub>- species, which represent carbon intermediates leading to CH<sub>4</sub>, were bonded to the catalyst surface in the smaller pores [19].

The olefins appeared to be the predominant primary products of these Fe-based catalysts in the FTS reaction. The C<sub>2-4</sub> selectivity obtained with the FeCuK/Q-50 was significantly higher than that with the FeCuK/Q-3 and

FeCuK/Q-10 catalysts, where increasing the pore size is beneficial for C<sub>2-4</sub> selectivity [4]. The formation of paraffin, which is produced from the secondary hydrogenation of olefins, was inhibited on the FeCuK/Q-50 catalyst as it had less Fe and a limited amount of Fe<sub>x</sub>C [20].

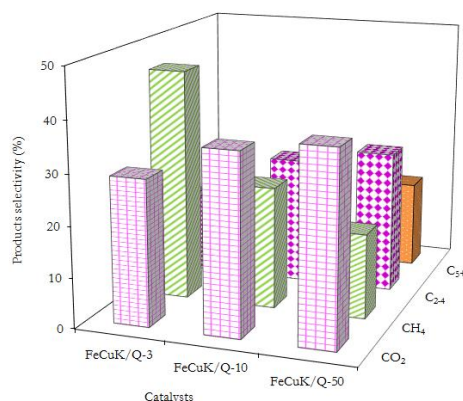


Fig. 8. Influence of the FeCuK/Q-3, FeCuK/Q-10, and FeCuK/Q-50 catalysts on the product selectivity in the 6-h FTS reaction. Reaction condition: 0.5 g catalyst, H<sub>2</sub>/CO of 1/1, 300 °C, 1.0 MPa, and a W/F of 10 g<sub>cat</sub> h/mol.

From Fig. 8, the FeCuK/Q-50 catalyst had the highest C<sub>2-4</sub> and, especially, C<sub>5+</sub> selectivity, supporting that larger pore sizes tended to be selective for the formation of heavy HCs [12] and an increased C<sub>5+</sub> selectivity. It is suggested that the dissociative adsorption of CO, which led to the formation of the CH<sub>2</sub> fragments required for chain growth, occurred in the larger pore sizes of silica [21].

## 4. Conclusions

The Fe-based catalysts containing Cu, K and citric acid and supported on different silica types were prepared by autocombustion for direct use in the FTS without a reduction step. In this study, the FTS performance of the catalysts were evaluated in a fixed-bed reactor at 300 °C, 1.0 MPa, W/F of 10 g<sub>cat</sub> h/mol, and H<sub>2</sub>/CO molar ratio of 1. The FeCuK/Q-50 catalyst produced the highest CO conversion level at 86.5% with 28.1% C<sub>2-4</sub> selectivity and 17.3% C<sub>5+</sub> selectivity under these operating conditions. Characterization of this catalyst by XRD and TEM analyses revealed the presence of Fe<sub>x</sub>C, which is known to be one of the Fe active phases. During the decomposition of citric acid, large amounts of gases, such as H<sub>2</sub>, CH<sub>4</sub>, H<sub>2</sub>O, CO, CO<sub>2</sub>, NH<sub>3</sub>, NO<sub>2</sub>, and NO, were released. The reducing H<sub>2</sub> and CO played a key role as the reducing and carburizing agents to produce Fe<sub>x</sub>C from the metal oxides phases. The larger crystallite sizes found in the large pores of the FeCuK/Q-50 catalyst were much easier to form Fe<sub>x</sub>C than the smaller crystallites in the small pores of FeCuK/Q-3 and FeCuK/Q-10. The pore sizes of the catalysts played a more important role than the surface area via influencing the formation of the Fe active phases and FTS performance. Of particular interest is that these Fe-based catalysts supported on different silica types derived from autocombustion do not require a reduction

step and provide another route to synthesize nanostructured metallic catalysts on silica for the production of clean biofuel for industry and transportations.

## Acknowledgement

This research is supported by Ratchadapisek Somphot Fund for Postdoctoral Fellowship, Chulalongkorn University, Thailand. The authors are grateful to Department of Applied Chemistry, School of Engineering, University of Toyama, Japan and Centre of Fuel and Energy from Biomass, Faculty of Science, Chulalongkorn University, Thailand for insight and equipment used in this work.

## References

- [1] Q. Zhang, J. Kang, and Y. Wang, "Development of novel catalysts for Fischer-Tropsch synthesis: tuning the product selectivity," *ChemCatChem*, vol. 2, pp. 1030-1058, 2010.
- [2] H. Suo, C. Zhang, B. Wu, J. Xu, Y. Yang, H. Xiang, and Y. Li, "A comparative study of Fe/SiO<sub>2</sub> Fischer-Tropsch synthesis catalysts using tetraethoxysilane and acidic silica sol as silica sources," *Catal. Today*, vol. 183, pp. 88-95, 2012.
- [3] O. O. James, A. M. Mesubi, T. C. Ako, and S. Maity, "Increasing carbon utilization in Fischer-Tropsch synthesis using H<sub>2</sub>-deficient or CO<sub>2</sub>-rich syngas feeds," *Fuel Process. Technol.*, vol. 91, pp. 136-144, 2010.
- [4] K. Cheng, M. Virginie, V. V. Ordonsky, C. Cordier, P. A. Chernavskii, M. I. Ivantsov, S. Paul, Y. Wang, and A. Y. Khodakov, "Pore size effects in high-temperature Fischer-Tropsch synthesis over supported iron catalysts," *J. Catal.*, vol. 328, pp. 139-150, 2015.
- [5] H. Suo, S. Wang, C. Zhang, J. Xu, B. Wu, Y. Yang, H. Xiang, and Y.-W. Li, "Chemical and structural effects of silica in iron-based Fischer-Tropsch synthesis catalysts," *J. Catal.*, vol. 286, pp. 111-123, 2012.
- [6] X. Guo, Y. Lu, P. Wu, K. Zhang, Q. Liu, and M. Luo, "The effect of SiO<sub>2</sub> particle size on iron based F-T synthesis catalysts," *Chin. J. Chem. Eng.*, vol. 24, pp. 937-943, 2016.
- [7] Z. Hua, Z. Cao, Y. Deng, Y. Jiang, and S. Yang, "Sol-gel autocombustion synthesis of Co-Ni alloy powder," *Mater. Chem. Phys.*, vol. 126, pp. 542-545, 2011.
- [8] L. Shi, K. Tao, T. Kawabata, T. Shimamura, X. J. Zhang, and N. Tsubaki, "Surface impregnation combustion method to prepare nanostructured metallic catalysts without further reduction: As-burnt Co/SiO<sub>2</sub> catalysts for Fischer-Tropsch synthesis," *ACS Catal.*, vol. 1, pp. 1225-1233, 2011.
- [9] S. Pengnarapat, P. Ai, P. Reubroycharoen, T. Vitidsant, Y. Yoneyama, and N. Tsubaki, "Active Fischer-Tropsch synthesis Fe-Cu-K/SiO<sub>2</sub> catalysts prepared by autocombustion method without a reduction step," *J. Energy Chem.*, vol. 27, pp. 432-438, 2018.
- [10] R. Phienluphon, L. Shi, J. Sun, W. Niu, P. Lu, P. Zhu, T. Vitidsant, Y. Yoneyama, Q. Chen, and N. Tsubaki, "Ruthenium promoted cobalt catalysts prepared by an autocombustion method directly used for Fischer-Tropsch synthesis without further reduction," *Catal. Sci. Technol.*, vol. 4, pp. 3099-3107, 2014.
- [11] R.-J. Liu, Y. Xu, Y. Qiao, Z.-H. Li, and X.-B. Ma, "Factors influencing the Fischer-Tropsch synthesis performance of iron-based catalyst: Iron oxide dispersion, distribution and reducibility," *Fuel Process. Technol.*, vol. 139, pp. 25-32, 2015.
- [12] Y. Zhang, J. Bao, S. Nagamori, and N. Tsubaki, "A new and direct preparation method of iron-based bimodal catalyst and its application in Fischer-Tropsch synthesis," *Appl. Catal. A Gen.*, vol. 352 pp. 277-281, 2009.
- [13] M. Rafati, L. Wang, and A. Shahbazi, "Effect of silica and alumina promoters on co-precipitated Fe-Cu-K based catalysts for the enhancement of CO<sub>2</sub> utilization during Fischer-Tropsch synthesis," *J. CO Util.*, vol. 12, pp. 34-42, 2015.
- [14] M. Ding, Y. Yang, B. Wu, Y. Li, T. Wang, and L. Ma, "Study on reduction and carburization behaviors of iron phases for iron-based Fischer-Tropsch synthesis catalyst," *Appl. Energy*, vol. 160, pp. 982-989, 2015.
- [15] R. Phienluphon, P. Ai, X. Gao, Y. Yoneyama, P. Reubroycharoen, T. Vitidsant, and N. Tsubaki, "Direct fabrication of catalytically active Fe<sub>x</sub>C sites by sol-gel autocombustion for preparing Fischer-Tropsch synthesis catalysts without reduction," *Catal. Sci. Technol.*, vol. 6, pp. 7597-7603, 2016.
- [16] K. Cheng, V. Subramanian, A. Carvalho, V. V. Ordonsky, Y. Wang, and A. Y. Khodakov, "The role of carbon pre-coating for the synthesis of highly efficient cobalt catalysts for Fischer-Tropsch synthesis," *J. Catal.*, vol. 337, pp. 260-271, 2016.
- [17] Ş. Özkara-Aydinoğlu, Ö. Ataç, Ö. F. Gül, Ş. Kınayyigit, S. Şal, M. Baranak, and İ. Boz, "α-olefin selectivity of Fe-Cu-K catalysts in Fischer-Tropsch synthesis: Effects of catalyst composition and process conditions," *Chem. Eng. J.*, vol. 181-182, pp. 581-589, 2012.
- [18] V. U. S. Rao, G. J. Stiegel, G. J. Cinquegrane, and R. D. Srivastava, "Iron-based catalysts for slurry-phase Fischer-Tropsch process: Technology review," *Fuel Process. Technol.*, vol. 30, pp. 83-107, 1992.
- [19] J. P. D. Breejen, P. B. Radstake, G. L. Bezemer, J. H. Bitter, V. Frøseth, A. Holmen, and K. P. D. Jong, "On the origin of the cobalt particle size effects in Fischer-Tropsch catalysis," *J. Am. Chem. Soc.*, vol. 131, pp. 7197-7203, 2009.
- [20] K. Kumabe, T. Sato, K. Matsumoto, Y. Ishida, and T. Hasegawa, "Production of hydrocarbons in

Fischer–Tropsch synthesis with Fe-based catalyst: Investigations of primary kerosene yield and carbon mass balance,” *Fuel*, vol. 89, pp. 2088-2095, 2010.

[21] L. Fan, K. Yokota, and K. Fujimoto, “Supercritical phase Fischer-Tropsch synthesis: Catalyst pore-size effect,” *AIChE J.*, vol. 38, pp. 1639-1648, 1992.



**Suthasinee Pengnarapat** received the B.Sc. degree in Chemistry and continued pursuing the M.Sc. degree in Petrochemistry and Polymer Science from Chulalongkorn University, Bangkok, Thailand. Prior to join in doctoral degree, she has worked in the petrochemistry industry as a scientist and an engineer. During Ph.D. study, she joined to Department of Applied Chemistry, University of Toyama, Japan for advanced project as researcher. For next two years, she received the Ph.D. degree in Petrochemistry and Polymer Science from Chulalongkorn University, Bangkok, Thailand.

Since July 2019, she has been a post-doctoral researcher with Chemical Technology, Faculty of Science, Chulalongkorn University, Bangkok, Thailand. Her research interests include Fischer-Tropsch synthesis (FTS), pyrolysis, gasification and biomass conversion.



**Tharapong Vitidsant** received the B.Sc. degree in Chemical Engineering from Chulalongkorn University, Bangkok, Thailand, the M.Sc. degree in Chemical Technology from Chulalongkorn University, Bangkok, Thailand, the D.E.A. in Chemical Engineering of ENISG and Dr.de L'INPT in Chemical Engineering of INPT, Toulouse, France.

He has worked at Department of Chemical Technology, Faculty of Science, Chulalongkorn University, Bangkok, Thailand and is currently a Professor. Also, he is head of Centre of Fuel and Energy from Biomass, Faculty of Science, Chulalongkorn University, Kaengkhroi, Saraburi, Thailand. He has the author of many books and articles and his research interests include reaction engineering, catalysis and heat transfer.

**Noritatsu Tsubaki**, photograph and biography not available at the time of publication

**Prasert Reubroycharoen**, photograph and biography not available at the time of publication

**Jaru Natakaranakul**, photograph and biography not available at the time of publication